Solid Phosphoric Acid Catalyst: A Multinuclear NMR and Theoretical Study

Thomas R. Krawietz, Ping Lin, Karen E. Lotterhos, Paul D. Torres, Dewey H. Barich, Abraham Clearfield, and James F. Haw*

Contribution from the Department of Chemistry, Texas A&M University, P.O. Box 300012, College Station, Texas 77842-3012

Received April 20, 1998

Abstract: The synthesis, structure, and acid function of solid phosphoric acid (SPA) catalyst were studied in detail. ^{31}P and ^{29}Si MAS NMR and X-ray powder diffraction identified the following crystalline silicon phosphate phases in SPA: $Si_5O(PO_4)_6$, *hexagonal*-SiP_2O_7, $Si(HPO_4)_2 \cdot H_2O$, and $SiHP_3O_{10}$. The acidity of SPA is due to a liquid or glassy solution of phosphoric acid oligomers supported on the silicon phosphate phases. ^{15}N MAS NMR of adsorbed pyridine-^{15}N and ^{13}C MAS NMR of adsorbed acetone-*2*-^{13}C showed Brønsted acid sites and no Lewis acid sites. $^{1}H \rightarrow {}^{15}N \rightarrow {}^{31}P$ and $^{1}H \rightarrow {}^{13}C \rightarrow {}^{31}P$ double cross polarization MAS NMR of the probe molecules provided a rare opportunity to use NMR to unambiguously localize chemisorption sites; the probe molecules are complexed to phosphoric acid and pyrophosphoric acid but not to the silicon phosphate phases. In situ NMR of the oligomerization of propene on SPA suggests that propene quantitatively reacts with phosphoric acid and its oligomers to form isopropyl phosphate, and formation of this very stable intermediate accounts for the lower olefin oligomerization activity of SPA relative to acidic zeolites. Theoretical calculations including geometries at B3LYP/6-311+G(d,p) and chemical shifts at GIAO-MP2/tzp/dz were used to model complexation of acetone or propene to SPA, and these support our conclusions.

The application of modern experimental and theoretical methods is providing an understanding of the structure and function of the solid acid catalysts used in chemical processes. Considerable progress has been made in the characterization and reaction chemistry of isolated Brønsted sites in aluminosilicate zeolites,[1−8] but less is known about other solid acid catalysts. Supported liquid-phase (SLP) catalysts are second only to zeolites in numbers of materials, processes, patents, and journal publications. SLP catalysts can be very straightforward materials, liquid acids dispersed on metal oxide supports.[9] But consider sulfuric acid dispersed on zirconia, sulfated zirconia.[10] This alkylation and cracking catalyst resists both characterization and consensus; there is little agreement regarding surface structure,[11] nature,[12] and strength of acidity,[13,14] and it has also been proposed that the acid function is incidental to a redox mechanism.[15]

For our first NMR and theoretical investigation of an SLP catalyst we selected solid phosphoric acid (SPA). This catalyst was developed in the 1930s and is used to this day in a number of processes including propene oligomerization and alkylation of benzene with propene to form cumene.[16−22] Remarkable for a highly successful solid acid catalyst, the literature reports no previous systematic investigation of SPA using modern spectroscopic or theoretical methods and especially no solid-state NMR studies. Here we report a thorough investigation of SPA using multinuclear NMR, X-ray powder diffraction, and ab initio theoretical methods. A large number of SPA samples were prepared with different synthesis conditions.[23−25]

We find that only ca. 60% of the phosphorus in SPA is present as free acids, and much of that is oligomerized. In agreement with previous reports,[23,24] we confirm the presence

* To whom correspondence should be addressed.

(1) Haw, J. F.; Nicholas, J. B.; Xu, T.; Beck, L. W.; Ferguson, D. B. *Acc. Chem. Res.* **1996**, *29*, 259−267.
(2) van Santen, R. A.; Kramer, G. J. *Chem. Rev.* **1995**, *95*, 637−660.
(3) Brändle, M.; Sauer, J. *J. Am. Chem. Soc.* **1998**, *120*, 1556−1570.
(4) Haase, F.; Sauer J. *J. Am. Chem. Soc.* **1995**, *117*, 3780−3789.
(5) Haw, J. F.; Xu, T.; Nicholas, J. B.; Goguen, P. W. *Nature* **1997**, *389*, 832−835.
(6) Goguen, P. W.; Xu, T.; Barich, D. H.; Skloss, T. W.; Song, W.; Wang, Z.; Nicholas, J. B.; Haw, J. F. *J. Am. Chem. Soc.* **1998**, *120*, 2650−2651.
(7) Blaszkowski, S. R.; van Santen, R. A. *J. Am. Chem. Soc.* **1996**, *118*, 5152−5153.
(8) Blaszkowski, S. R.; van Santen, R. A. *J. Am. Chem. Soc.* **1997**, *119*, 5020−5027.
(9) Villadsen, J.; Livbjerg, H. *Catal. Rev.-Sci. Eng.* **1978**, *17*, 203−272.
(10) Song, X.; Sayari, A. *Catal. Rev.-Sci. Eng.* **1996**, *38*, 329−412.
(11) Adeeva, V.; de Haan, J. W.; Janchen, J.; Lei, G. D.; Schunemann, V.; van de Ven, L. J. M.; Sachtler, W. M. H.; van Santen, R. A. *J. Catal.* **1995**, *151*, 364−372.
(12) Clearfield, A.; Serrette, G. P. D.; Khazi-Syed, A. H. *Catal. Today* **1994**, *20*, 295−312.
(13) Hino, M.; Kobayashi, S.; Arata, K. *J. Am. Chem. Soc.* **1979**, *101*, 6439−6441.
(14) Tabora, J. E.; Davis, R. J. *J. Am. Chem. Soc.* **1996**, *118*, 12240−12241.
(15) Farcasiu, D.; Ghenciu, A.; Li, J.-Q. *J. Catal.* **1996**, *158*, 116−127.
(16) (a) Ipatieff, V. U.S. Patent No. 1,993,512, 1935. (b) Ipatieff, V. U.S. Patent No. 1,993,513, 1935.
(17) Ipatieff, V.; Schaad, R. E. U.S. Patent No. 2,275,182, 1942.
(18) Ipatieff, V.; Schaad, R. E. U.S. Patent No. 2,157,208, 1939.
(19) McMahon, J. F.; Bednars, C.; Solomon, E. *Adv. Pet. Chem. Refin.* **1963**, *7*, 284−321.
(20) Jones, E. K. *Adv. Catal.* **1956**, *8*, 219−238.
(21) Weisang, E.; Engelhard, P. A. *Bull. Soc. Chim. Fr.* **1968**, 1811−1820.
(22) Oblad, A. G.; Mills, G. A.; Heinemann, H. In *Catalysis*; Emmett, Ed.; Reinhold: New York, 1958; Vol. VI, pp 341−406.
(23) Durand, B.; Lenzi, M.; Boullé, A. *Bull. Soc. Chim. Fr.* **1972**, *2*, 442−456.
(24) Cavani, F.; Girotti, G.; Terzoni, G. *Appl. Catal. A: Gen.* **1993**, *97*, 177−196.
(25) Ipatieff, V. N.; Schaad, R. E.; Shaney, W. B. *Catalytic Polymerization of Olefins*; Oxford University Press: London, 1953; Vol. V, Part II.

S0002-7863(98)01346-8 CCC: $15.00
Published on Web 08/05/1998

of crystalline silicon orthophosphate ($Si_5O(PO_4)_6$) and hexagonal silicon pyrophosphate (SiP_2O_7) in SPA. We extend the identification of silicon phosphates in SPA to include silicon hydrogen phosphate monohydrate ($Si(HPO_4)_2 \cdot H_2O$)[26,27] and silicon hydrogen tripolyphosphate ($SiHP_3O_{10}$).[26] We also synthesized the silicon phosphates as either pure or majority phases and surveyed their NMR behavior, which is exceptional due to the presence of octahedral silicon in these phases.

The nature and strength of the acid sites on SPA was investigated by measuring the NMR spectra of common probe molecules and in situ NMR[1,28] of propene oligomerization.[29] Propene oligomerization on SPA occurs at much higher temperatures than on zeolite acid catalysts, because it first reacts with phosphoric acid to form isopropyl phosphate. The probe molecule studies reveal that all of the acid sites on SPA are Brønsted; there are no Lewis sites. $^1H \rightarrow ^{15}N \rightarrow ^{31}P$ and $^1H \rightarrow ^{13}C \rightarrow ^{31}P$ double cross polarization experiments prove that the basic probe molecules are complexed to phosphoric acid and its oligomers. The chemical shift of acetone is larger on SPA than on zeolite HZSM-5, suggesting that SPA is the stronger acid. This interpretation is counter to the conventional ordering of acid strengths based on propene oligomerization activity. Quantitative conversion of propene to isopropyl phosphate on SPA accounts for the difference in oligomerization activity on the two media. We used theoretical methods to better understand the acid strength of SPA. We optimized a number of geometries of acetone or propene complexed to species known to be present in SPA and then calculated theoretical chemical shift tensors. These calculations provide several lines of evidence that the acid strength of SPA is greater than that of zeolites.

Experimental Section

Materials. Pyridine-^{15}N (98+% ^{15}N), acetone-*2*-^{13}C (99% ^{13}C), and 5.8 N ammonium-^{15}N hydroxide (98% ^{15}N) were purchased from Cambridge Isotopes. Propene-*1*-^{13}C (99% ^{13}C) and propene-*2*-^{13}C (99% ^{13}C) were purchased from CDN Isotopes. Ammonium-^{15}N nitrate (99% ^{15}N) was purchased from MSD Isotopes. 2-Propanol-*2*-^{13}C (99% ^{13}C) was purchased from Isotec. Kieselgühr (91.9% SiO_2), electronic grade silicon(IV) oxide (Puratrem, 99.999%), sodium hexafluorosilicate (99%), and (2*S*,3*S*)-chiraphos (99%) were purchased from Strem Chemicals. Hexamethylbenzene (HMB), H_3PO_4 (98%), pyrophosphoric acid (85+%), and acetone (spectrophotometric grade, 99.5%) were purchased from Aldrich. H_3PO_4 (85%) and phosphorus pentoxide (99%) were purchased from EM Science. Ammonium-^{15}N dihydrogen phosphate was synthesized from the dropwise addition of 5.0 g of 5.8 N ammonium-^{15}N hydroxide to an ice-cooled solution of 3.34 g of 85% phosphoric acid diluted in 10 mL of deionized water. The water was evaporated on a stirred hot plate, and the remaining solid was dried in an oven at 423 K.

Acid-washed kieselgühr was prepared with 10 mL of 0.1 M HCl/g of kieselgühr to remove excess Fe_2O_3. The slurry was then filtered and dried at 473 K. This procedure was carried out a total of three times. Following acid leaching, the kieselgühr contained 0.65 wt % Fe, as determined by ICP/AE (Galbraith Labs).

Silicon Phosphate Synthesis. Crystalline silicon phosphates were synthesized with 85% phosphoric acid and either acid-washed kieselgühr or electronic grade silicon(IV) oxide as sources of phosphate and silica, respectively. The silica source was dried in air at 473 K prior to use. After preparation, all materials were immediately ground with quartz coated ceramic utensils and sealed to prevent adsorption of atmospheric moisture.

With the exception of $SiHP_3O_{10}$, the crystalline components of SPA were synthesized in >95% purity, as measured by quantitative ^{31}P MAS NMR. $Si_5O(PO_4)_6$ was synthesized by heating an evacuated quartz ampule containing 5.0 g of silica and 11.8 g of phosphorus pentoxide to 858 K for 24 h. $Si(HPO_4)_2 \cdot H_2O$ was prepared by heating a slurry of 5.0 g of silica and 19.2 g of 85% phosphoric acid to 473 K in a shallow-form dish for 336 h. The hexagonal polymorph of SiP_2O_7 was prepared by heating a mixture of 5.0 g of silica with 28.8 g of 85% phosphoric acid to 873 K for 48 h. ^{31}P and ^{29}Si MAS NMR and powder XRD were used to confirm the identity and purity of each silicon phosphate phase.

SPA catalyst samples were prepared in 70 mL of shallow-form, quartz-coated alumina dishes (Coors) from viscous pastes consisting of 5.0 g of silica and 28.8 g of 85% phosphoric acid (Si:P mol ratio of 1.0:3.0). This mixture was heated to 573 K for 48 h to form "as-prepared SPA".

Cold water washes of SPA catalyst were used to remove phosphoric acid and oligomerized phosphoric acids without hydrolysis of silicon phosphate phases. Typically, 10 mL of deionized water/g of catalyst was vigorously stirred for 10 min, followed by vacuum filtration and drying the resultant solid in an oven at 473 K for 10 min. ^{31}P MAS NMR showed that >98% of phosphoric acid is removed from the catalyst without degradation of the silicon phosphate phases.

NMR Spectroscopy. ^1H, ^{13}C, ^{15}N, ^{29}Si, and ^{31}P MAS NMR spectra were obtained on either a Chemagnetics CMX-360 or a home-built 200 MHz instrument. All spectra were externally referenced with acetone (^1H, 2.11 ppm relative to ^1H in tetramethylsilane), HMB (^{13}C, methyl at 17.4 ppm relative to ^{13}C in tetramethylsilane), ammonium-^{15}N nitrate (^{15}N, ammonium at −359 ppm relative to ^{15}N in nitromethane), sodium hexafluorosilicate (^{29}Si, −188.6 ppm relative to ^{29}Si in tetramethylsilane), or (2*S*,3*S*)-chiraphos (^{31}P, upfield resonance at −13.3 ppm relative to 85% phosphoric acid). All Bloch decay spectra reported used quantitative conditions. $^1H \rightarrow ^{13}C \rightarrow ^{31}P$ and $^1H \rightarrow ^{15}N \rightarrow ^{31}P$ double cross polarization spectra were acquired at 198 K on a triple resonance probe from Otsuka Electronics spinning 7.5 mm zirconia rotors. All spectra presented used active spin speed control.

X-ray Diffraction. X-ray powder diffraction patterns of silicon phosphates were obtained on a Seifert-Scintag PAD V automated diffractometer with Cu K_α radiation. The X-ray source was an anode operating at 40 kV and 30 mA with a copper target and filtered with nickel foil ($\lambda = 1.5418$ Å). Data were collected between 5° and 62° in 2θ with a step size of 0.04°. The scan rate was 2.4 s/step. The measured X-ray diffraction patterns were compared with those reported in the JCPDS database.

Computations. All structures were fully optimized with density functional theory (DFT) with use of the 6-311+G(d,p) basis set. Becke's three-parameter hybrid method,[30] using the LYP correlation functional,[31] was used in all DFT calculations. Harmonic frequency analyses were performed on geometries optimized at the B3LYP/6-31G(d) level of theory with use of analytical second derivatives.

The method of gauge-invariant atomic orbitals (GIAO)[32,33] was used for chemical shift calculations. We used Alrich's[34] tzp {51111/311/1} (with 6 Cartesian d orbitals) on carbon and oxygen atoms, tzp {5121111/51111/1} on phosphorus, and dz {31} on the hydrogens in all of the chemical shift calculations. ^{13}C chemical shifts were calculated at the GIAO-RHF/tzp/dz level of theory and referenced against tetramethylsilane calculated at the same level. All of the above calculations were performed within the Gaussian 94 program package.[35] For small clusters, we also performed chemical shift calculations at the GIAO-MP2/tzp/dz level of theory[36] with ACES II.[37]

Results

^{31}P and ^{29}Si MAS NMR of SPA Catalysts. We first studied catalyst samples synthesized using kieselgühr as the silica source

(26) Lelong, B. *Ann. Chim.* **1964**, *9*, 229−260.
(27) Mudrakovskii, I. L.; Mastikhin, V. M.; Shmachkova, V. P.; Kotsarenko, N. S. *Chem. Phys. Lett.* **1985**, *120*, 424−426.
(28) Xu, T.; Haw, J. F. *Top. in Catal.* **1997**, *4*, 109−118.
(29) Haw, J. F.; Richardson, B. R.; Oshiro, I. S.; Lazo, N. L.; Speed, J. A. *J. Am. Chem. Soc.* **1989**, *111*, 2052−2058.
(30) Becke, A. D. *J. Chem. Phys.* **1993**, *98*, 5648−5652.
(31) Lee, C.; Yang, W.; Parr, R. G. *Phys. Rev. B* **1988**, *37*, 785−789.
(32) Ditchfield, R. *Mol. Phys.* **1974**, *27*, 789−807.
(33) Wolinski, K.; Hinton, J. F.; Pulay, P. *J. Am. Chem. Soc.* **1990**, *112*, 8251−8260.
(34) Schafer, A.; Huber, C.; Ahlrichs, R. *J. Chem. Phys.* **1992**, *100*, 5829−5835.

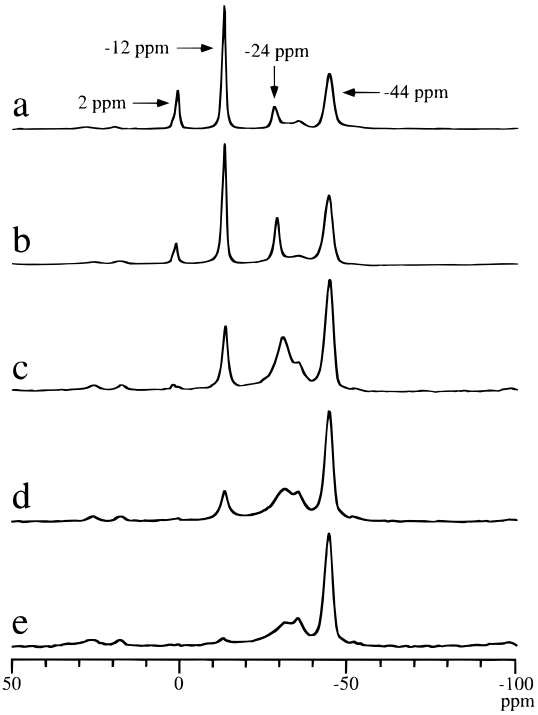

Figure 1. 80.8 MHz ^{31}P MAS Bloch decay spectra of SPA samples heated under vacuum for 2 h at the indicated temperature: (a) 298, (b) 413, (c) 453, (d) 493, (e) 533 K. All spectra were acquired at 298 K and are the result of 12 transients utilizing a 60 s recycle delay and a spinning speed of 5000 Hz. See text for assignments.

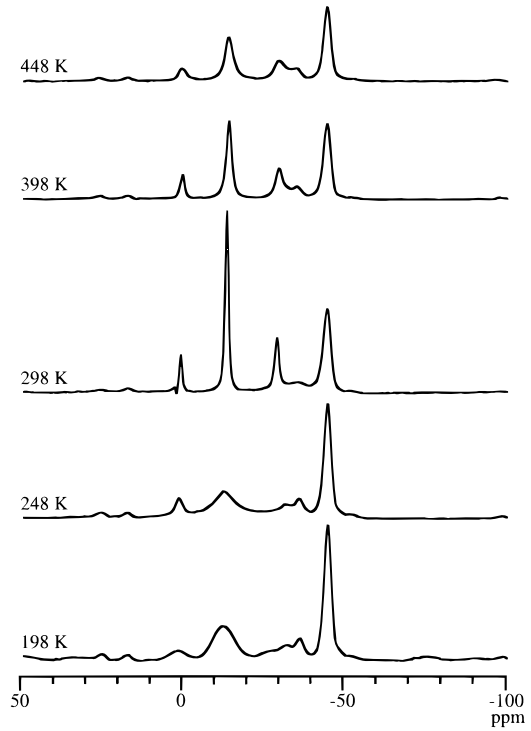

Figure 2. 80.8 MHz variable-temperature ^{31}P MAS Bloch decay spectra of a SPA sample evacuated at 373 K for 2 h. Phosphoric acid (ca. 2 ppm) and oligomerized acids (−12 and −24 ppm) are in a glassy state at 248 K and below, and in a solution state at higher temperatures. Broadening at the highest temperatures studied may reflect chemical exchange. All spectra are the result of 12 transients utilizing a 60 s recycle delay and a spinning speed of 5000 Hz.

as in industrial preparations.[16,17] At 298 K several of the ^{31}P resonances were greater than 10 ppm in width, and those assigned to phosphoric acid and its oligomers broadened with increasing temperature so as not to be detected at 398 K and above. The total integrated intensity of the MAS spectra strongly deviated from the Curie law at higher temperatures. Elemental analysis showed that SPA prepared with kieselgühr contained 3600 ppm iron. We observed similar temperature-dependent ^{31}P NMR line widths for a 0.036 M $FeCl_3$ (3400 ppm Fe^{3+}) solution in 85% H_3PO_4. To obtain NMR results free of paramagnetic broadening, we synthesized SPA samples using high purity, electronic grade silicon(IV) oxide. X-ray powder diffraction (vide infra) showed that the crystalline phases were identical for catalysts prepared from either silica source, and other than paramagnetic broadening, the NMR results were identical as well. All NMR results for SPA catalysts reported below were obtained with use of electronic grade silicon(IV) oxide.

Figure 1 shows ^{31}P MAS spectra measured at 298 K for five catalysts that were heated under vacuum at various temperatures prior to sealing in MAS rotors under an anhydrous N_2 atmosphere. Processes using SPA require careful control of the water content in the feed,[9,24] and the large changes in the downfield signals in the NMR spectra as a function of drying conditions motivate the molecular-level interpretation of this effect. These downfield signals are due to phosphoric acid (ca. 2 ppm), terminal (−12 ppm), and internal (−24 ppm) phosphate groups in phosphoric acid oligomers.[38] These assignments were confirmed by solution NMR studies of washes of the catalyst samples with anhydrous ethanol, MAS NMR studies of solid 98% H_3PO_4 and pyrophosphoric acid, and other standard procedures. The average chain length of the phosphoric acid species on the catalysts, $\mathbf{n}_{av}$, can be determined from the integrated intensities of the three signals:

$$\mathbf{n}_{av} = (\mathbf{A}_{H_3PO_4} + \mathbf{A}_{term.} + \mathbf{A}_{intern.})/(\mathbf{A}_{H_3PO_4} + 0.5\mathbf{A}_{term.})$$

As-prepared SPA has an average chain length of 2.0 (pyrophosphoric acid) and samples evacuated at 453 K and above have average chain lengths approaching 3.0 (tripolyphosphoric acid). The concentrations of very strong phosphoric acid solutions are commonly reported on a percent P_2O_5 basis, and the acidic phase of as-prepared SPA corresponds to approximately 80% P_2O_5.

Figure 2 reports variable-temperature ^{31}P MAS spectra of an SPA sample that was treated by evacuation at 373 K. The signals due to phosphoric acids broaden considerably at temperatures below 298 K. The pure acids are low-melting solids (e.g., 100% H_3PO_4 melts at 315 K), and mixtures of phosphoric and pyrophoshoric acids are viscous liquids at 298 K. The low-temperature NMR behavior in Figure 2 is consistent with the freezing out of various conformations and intermolecular interactions as in polymers below their glass transitions. Residual dipolar broadening is also a potential contributor to line broadening at reduced temperature. The signals due to

(35) Gaussian 94, Revision E.2. Frisch, M. J.; Trucks, G. W.; Schlegel, H. B.; Gill, P. M. W.; Johnson, B. G.; Robb, M. A.; Cheeseman, J. R.; T. Keith; Petersson, G. A.; Montgomery, J. A.; Raghavachari, K.; Al-Laham, M. A.; Zakrzewski, V. G.; Ortiz, J. V.; Foresman, J. B.; Cioslowski, J.; Stefanov, B. B.; Nanayakkara, A.; Challacombe, M.; Peng, C. Y.; Ayala, P. Y.; Chen, W.; Wong, M. W.; Andres, J. L.; Replogle, E. S.; Gomperts, R.; Martin, R. L.; Fox, D. J.; Binkley, J. S.; Defrees, D. J.; Baker, J.; Stewart, J. P.; Head-Gordon, M.; Gonzalez, C.; Pople, J. A.; Pittsburgh, PA, 1995.

(36) Gauss, J. *Chem. Phys. Lett.* **1992**, *191*, 614−620.

(37) ACES II, an ab initio quantum chemical program system: Stanton, J. F.; Gauss, J.; Watts, J. D.; Lauderdale, W. J.; Bartlett, R. J.

(38) Crutchfield, M. M.; Callis, C. F.; Irani, R. R.; Roth, G. C. *Inorg. Chem.* **1962**, *1*, 813−817.

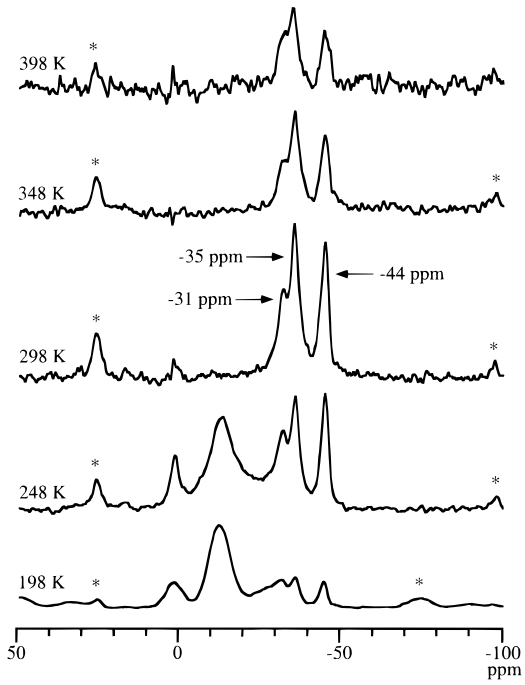

Figure 3. 80.8 MHz variable-temperature ^{31}P CP MAS spectra of a SPA sample evacuated at 373 K for 2 h. Relative cross polarization efficiencies, estimated by the comparison of these spectra with the corresponding Bloch decay spectra (cf., Figure 2), reflect both the presence or absence of protons and the extent of dynamical averaging. All spectra are the result of 64 transients with a 1 ms ^{1}H→^{31}P contact time utilizing a 10 s recycle delay and a spinning speed of 5000 Hz. Asterisks denote spinning sidebands.

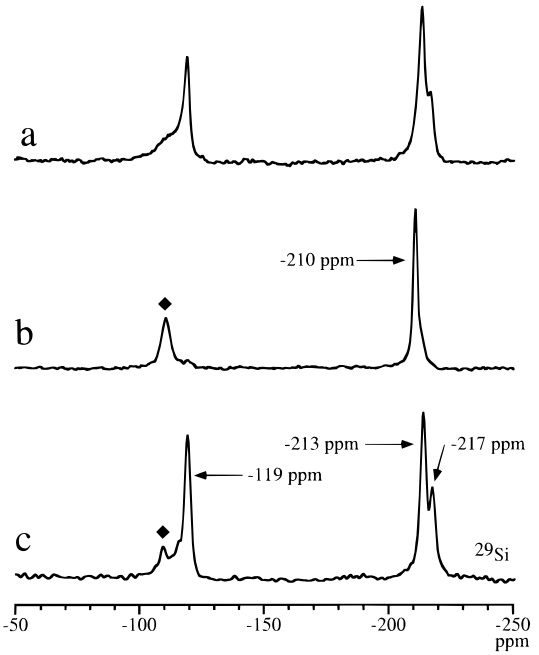

Figure 4. 71.5 MHz ^{29}Si MAS Bloch decay spectra. (a) SPA contains silicon in both tetrahedral (−119 ppm) and octahedral (ca. −210 to −217 ppm) environments. (b) $Si(HPO_4)_2{\cdot}H_2O$ contains only octahedrally coordinated silicon at −210 ppm. Unreacted silica (◆) is also present at −109 ppm. (c) $Si_5O(PO_4)_6$ shows isotropic peaks at −119, −213, and −217 ppm in the 2:2:1 intensity ratio predicted from the crystal structure. Quantitative ^{29}Si spectra in each case required 256 transients and a 20 s recycle delay. All spectra were acquired with a spinning speed of 5000 Hz.

phosphoric acids also broaden above 448 K; possible dynamics at high temperatures may include chemical exchange of phosphate units between various oligomers, but we did not investigate this any further.

The upfield signals in Figures 1 and 2 are due to crystalline silicon phosphate phases formed by chemical reaction between phosphoric acid and silica. The evidence for these assignments is described below. These signals are due to silicon orthophosphate ($Si_5O(PO_4)_6$, −44 ppm) and smaller amounts of silicon hydrogen phosphate monohydrate ($Si(HPO_4)_2{\cdot}H_2O$, −31 ppm) and silicon hydrogen tripolyphosphate ($SiHP_3O_{10}$, −35 ppm). A very small amount (typically <1%) of hexagonal silicon pyrophosphate (SiP_2O_7, −52 ppm) can also be observed in the ^{31}P MAS spectra of many SPA samples.

The structure and dynamics of the components of SPA catalyst are also reflected in the signal intensities observed in ^{1}H→^{31}P cross polarization spectra (Figure 3). The signals due to phosphoric acids effectively cross polarize only at low temperatures; at 298 K and above these species are in a liquidlike environment. The relative cross polarization efficiencies of the various silicon phosphate phases reflect the presence or absence of protons; thus, the signals due to $Si(HPO_4)_2{\cdot}H_2O$ and $SiHP_3O_{10}$ are greatly emphasized relative to the quantitative Bloch decay spectra (Figure 2) and the peak at −44 ppm due to $Si_5O(PO_4)_6$ is by comparison attenuated. The latter phase must contain *some* hydrogen as impurities or inclusions; otherwise there would be no cross polarization response, as we observe for the pure compound.

Using X-ray powder diffraction measurements, other workers have previously reported that SPA contains silicon orthophosphate ($Si_5O(PO_4)_6$).[23,24] A careful examination of our X-ray powder data on SPA samples suggested other specific silicon phosphate phases, which we then synthesized as pure or majority phases for NMR characterization. Figure 4 reports ^{29}Si MAS NMR spectra of our preparations of SPA, silicon hydrogen phosphate monohydrate, ($Si(HPO_4)_2{\cdot}H_2O$), and silicon orthophosphate, ($Si_5O(PO_4)_6$); the ^{29}Si spectra are also compared with that of a SPA sample. A similar procedure yielded the $SiHP_3O_{10}$ assignment. The upfield ^{29}Si chemical shifts (ca. 210−220 ppm in Figure 4) are from *octahedrally coordinated silicon.*[39] For example, Clearfield and co-workers previously used powder methods to solve the crystal structure of $Si_5O(PO_4)_6$ and determined that the unit cell contains five silicon atoms: two equivalent tetrahedral sites, two equivalent octahedral sites, and a second octahedral site.[40] The ^{29}Si spectrum of $Si_5O(PO_4)_6$ is thus completely assigned by comparison to the crystal structure.

Silicon pyrophosphate (SiP_2O_7) is a minority species in SPA, but its characterization caused us a disproportionate amount of trouble due to the existence of a number of polymorphs.[41−45] We synthesized pure samples of the four well-established polymorphs and found that their ^{31}P spectra (Figure 5) were in agreement with their solved crystal structures. Our NMR work has found only the hexagonal polymorph of SiP_2O_7 in SPA. Principal components of the ^{31}P chemical shift tensors were determined by the method of Herzfeld and Berger[46] for most

(39) Weeding, T. L.; de Jong, B. H. W. S.; Veeman, W. S.; Aitken, B. G. *Nature* **1985**, *318*, 352−353.
(40) Poojary, D. M.; Borade, R. B.; Clearfield, A. *Inorg. Chim. Acta* **1993**, *208*, 23−29.
(41) Bissert, G.; Liebau, F. *Naturwissenschaften* **1969**, *56*, 212.
(42) Poojary, D. M.; Borade, R. B.; Campbell, F. L., III; Clearfield, A. *J. Solid State Chem.* **1994**, *112*, 106−112.
(43) Liebau, F.; Bissert, G.; Koppen, N. *Z. Anorg. Allg. Chem.* **1968**, *359*, 113−134.
(44) Makart, H. *Helv. Chim. Acta* **1967**, *50*, 399−405.
(45) Hartmann, P.; Jana, C.; Vogel, J.; Jäger, C. *Chem. Phys. Lett.* **1996**, *258*, 107−112.
(46) Herzfeld, J.; Berger, A. E. *J. Chem. Phys.* **1980**, *73*, 6021−6030.

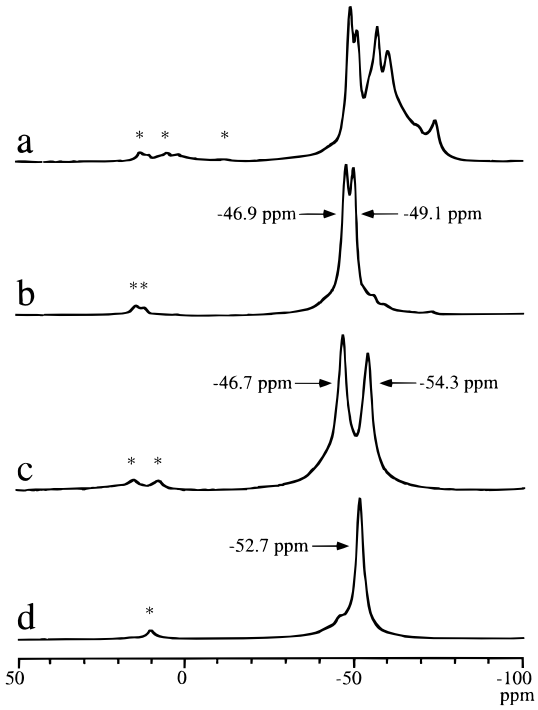

Figure 5. 80.8 MHz ^{31}P MAS Bloch decay spectra of four polymorphs of SiP_2O_7. In each case the parenthetical information denotes reaction temperature, reaction time, and initial Si:P molar ratio. (a) *cubic*-SiP_2O_7 (1273 K, 4 h, 1.0:3.0) shows that many of the 11 crystallographically distinct phosphorus nuclei are resolved. (b) *monoclinic*-SiP_2O_7 (1273 K, 4 h, 1.0:4.0) shows two resonances at −46.9 and −49.1 ppm. (c) *tetragonal*-SiP_2O_7 (973 K, 4 h, 1.0:1.0) shows two resonances at −46.7 and −54.3 ppm. (d) *hexagonal*-SiP_2O_7 (773 K, 48 h, 1.0:3.0) shows a single resonance at −52.7 ppm. Each spectrum is the result of 512 transients utilizing a 2 s recycle delay and a spinning speed of 5000 Hz. Asterisks denote spinning sidebands.

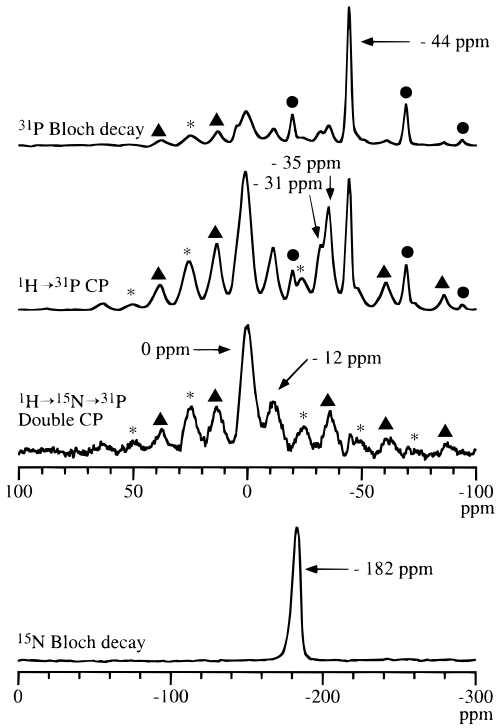

Figure 6. 36.5 MHz ^{15}N MAS and 145.6 MHz ^{31}P MAS spectra of a SPA sample evacuated at 298 K followed by adsorption of 1.6 mmol/g pyridine-^{15}*N*. The ^{15}N MAS spectrum (298 K shown) has a single resonance at −182 ppm, indicative of coordination to a Brønsted site. We used the ^{15}N spin on pyridine as means of determining which phosphorus atoms in the catalyst were close in space to the adsorbed base. To obtain efficient ^{1}H→^{15}N→^{31}P double cross polarization (4 ms ^{1}H→^{15}N contact, 6 ms ^{15}N→^{31}P contact), we measured the ^{31}P MAS NMR spectra at 153 K using a spinning speed of 3600 Hz. This experiment shows unambiguously that the pyridine is complexed to phosphoric acid and its oligomers, not to the silicon phosphate phases. ^{1}H→^{31}P cross polarization and ^{31}P Bloch decay spectra acquired under similar conditions are shown for comparison. ★, ▲, and ● denote spinning sidebands of phosphoric acid, terminal groups of oligomerized acid, and silicon orthophosphate, respectively.

of the silicon phosphate phases and are reported in the Supporting Information.

NMR Characterization of Acid Sites and Reaction Mechanism. The above structural characterization of SPA suggests little potential for Lewis sites on this catalyst; nevertheless, there are anecdotal accounts of Lewis acidity for silicon phosphates. We investigated this hypothesis using the ^{15}N MAS spectrum of adsorbed pyridine[47] as a profile of SPA acidity. We studied a number of samples with various pyridine loadings and measured the ^{15}N spectra over a range of temperatures to guard against dynamical averaging. The pyridine studies revealed only Brønsted sites and no evidence of Lewis sites. Pyridine-^{15}*N* on SPA provides the NMR spectroscopist an unusually straightforward opportunity to locate an adsorbate molecule on a complex heterogeneous catalyst. Figure 6 reports various CP/MAS spectra measured at 153 K of a sample of 1.6 mmol/g of pyridine-^{15}*N* on a SPA sample prepared by evacuation at 298 K for 30 min. In these spectra the spinning speed was deliberately set to a low value, 3600 Hz, to improve cross polarization efficiency, with the consequence that the ^{31}P MAS spectra are crowded with spinning sidebands. Nevertheless, the isotropic ^{31}P signals for phosphoric acid (ca. 0 ppm), terminal phosphates (−12 ppm), and several silicon phosphate phases are clearly resolved. Quantitative ^{15}N Bloch decay MAS NMR shows that all of the pyridine is protonated (−182 ppm).[48] Figure 6 also reports the ^{1}H→^{15}N→^{31}P double cross polarization spectrum of this sample. Cross polarization is a "through space" method of polarization transfer, and its rate is highly dependent upon distance. The double cross polarization spectrum is expected to report only those ^{31}P spins that are within a few angstroms of a ^{15}N spin. Indeed, only phosphoric acids are observed when the magnetization is transferred though pyridine. The adsorbed base is not associated with the silicon phosphate phases.

Most of the processes that use SPA convert propene into other products. This olefin and associated intermediates and products have been the subject of detailed in situ NMR studies of reactions on zeolites and metal halide acids.[29,49] Propene is readily adsorbed into the channel structures of zeolites, even at the lowest temperatures. On acidic zeolites, propene forms a π complex with the Brønsted site at cryogenic temperatures, which is observed as a downfield shift of the C-2 resonance. The zeolite studies also show that propene reversibly forms a framework bound isopropoxyl species below room temperature.[29,49] This process results in 1, 3 ^{13}C label scrambling, but not 1, 2, 3 ^{13}C scrambling as is seen on frozen superacids[50]

(47) Haw, J. F.; Chuang, I.-S.; Hawkins, B. L.; Maciel, G. E. *J. Am. Chem. Soc.* **1983**, *105*, 7206−7207.
(48) Xu, T.; Kob, N.; Drago, R. S.; Nicholas, J. B.; Haw, J. F. *J. Am. Chem. Soc.* **1997**, *119*, 12231−12239.
(49) Nicholas, J. B.; Xu, T.; Haw, J. F. *Top. Catal.* **1998**, *6*, 141−149.
(50) Nicholas, J. B.; Xu, T.; Barich, D. H.; Torres, P. D.; Haw, J. F. *J. Am. Chem. Soc.* **1996**, *118*, 4202−4203.

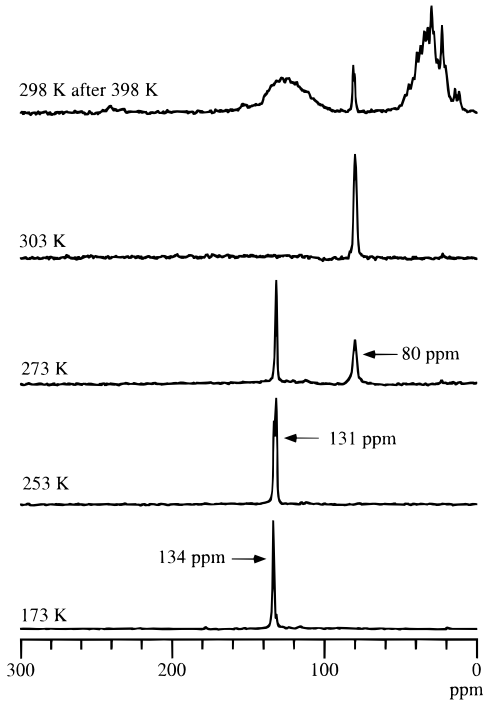

Figure 7. 90.5 MHz ^{13}C in situ MAS NMR study of the reactions of propene-*2*-^{13}*C* on a sample of SPA prepared by evacuation at 373 K followed by adsorption at 153 K. Propene is excluded from the catalyst at low temperatures, and reacts with the catalyst to form isopropyl phosphate (C-2 at 80 ppm) at 273 K and above. Oligomerization occurs at 398 K.

that reversibly form a free isopropyl carbenium ion. On zeolites propene oligomerizes in the vicinity of room temperature; on SPA propene oligomerization occurs at higher temperatures. This has been used to argue that SPA is a weaker acid than zeolites.

We carried out a number of in situ NMR studies of propene oligomerization on SPA using methods very similar to our zeolite studies. Figure 7 reports representative results from in situ studies of propene-*2*-^{13}*C* on SPA prepared by evacuation at 373 K. A signal at 134 ppm is observed for propene on SPA at low temperature; this is almost identical to the solution or gas-phase value. For comparison, a chemical shift of 146 ppm was observed for π complexes of propene on zeolite HZSM-5. We carried out a number of experiments to establish the environment of unreacted propene on SPA at low temperatures; for example, we observed no spinning sidebands and little cross polarization efficiency. We conclude that propene is not dissolved into the glassy phosphoric acid phase at low temperature. At 273 K propene began to react with the catalyst to form isopropyl phosphate. This reaction was complete at 298 K. The phosphate ester was very mobile at 298 K, but when the sample was cooled to 173 K, we readily observed spinning sidebands and a strong cross polarization response for this species. Similar in situ experiments with propene-*1*-^{13}*C* (not shown) established that propene does not undergo 1, 3 ^{13}C label scrambling prior to formation of isopropyl phosphate, as is the case for the reversible formation of surface-bound alkoxyl species in zeolites. The irreversible nature of isopropyl phosphate formation at these low temperatures also underscores the stability of this species. The ester is indefinitely stable on SPA at moderate temperatures, but it reacts at approximately 398 K to yield a complex mixture of products characteristic of "conjunct polymerization". The complex mixture of reaction products generated is a result of the long reaction times in an

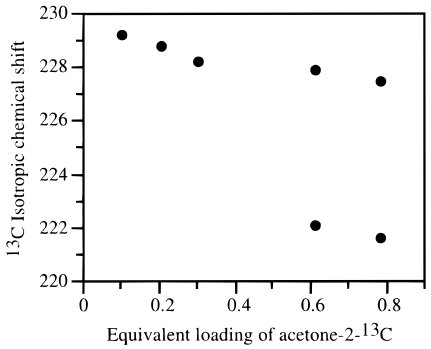

Figure 8. Summary of loading-dependent ^{13}C isotropic chemical shifts of the carbonyl carbon of acetone-*2*-^{13}*C* on a SPA sample prepared by evacuation at 298 K. Measurements were performed at 153 K to obtain spectra in the slow-exchange regime. Equivalent loading is defined as the ratio of acetone molecules to phosphate units in phosphoric acid and its oligomers.

NMR study carried out in a sealed rotor. In some in situ experiments (not shown) we observed low concentrations of free propene immediately prior to the onset of oligomerization. This presumably reflects the decomposition of isopropyl phosphate at higher temperatures.

Acetone-*2*-^{13}*C* is widely applied as a probe molecule for the study of solid acids.[48,51] In the case of Brønsted sites on zeolites, the shift is commonly interpreted in terms of conventional notions of relative acid strength. For the case of zeolite HZSM-5, a strongly acidic zeolite, this value is ca. 223 ppm. We observed that acetone has a shift of 228.5 ppm when a very low loading is adsorbed on SPA evacuated at 298 K, and values as high as 231 ppm were obtained for samples evacuated at higher temperatures. On solid 98% H_3PO_4 and solid 85+% pyrophosphoric acid, we found acetone shifts of 228.1 and 229.8 ppm, respectively.

The possibility of a role for the crystalline components in the downfield shifts observed for acetone on SPA was ruled out by several experiments. We used a literature procedure[24] to remove the phosphoric acid component of SPA with cold water washings followed by drying and observed that acetone has a chemical shift of only 213 ppm on such materials. The distance dependence of magnetization transfer by cross polarization was exploited to establish unambiguously that basic probe molecules on SPA are complexed to phosphoric acid species and are not associated with the mineral phases. ^{1}H→^{13}C→^{31}P double cross polarization experiments were carried out for acetone-*2*-^{13}*C* on SPA. These were analogous to the ^{1}H→^{15}N→^{31}P double cross polarization experiments with pyridine-^{15}*N* reported in Figure 6. The ^{1}H→^{13}C→^{31}P experiments (reported in the Supporting Information) show that acetone on SPA is complexed to phosphoric acid species and is not associated with the silicon phosphate phases.

We explored the loading dependence of the ^{13}C isotropic shift of acetone on SPA evacuated at 298 K (Figure 8) and found, not surprisingly, that SPA has a distribution of apparent acid strength, especially at higher loadings. ^{13}C NMR measurements were performed at 153 K to eliminate chemical exchange between acetone in different coordination environments. At lower loadings, there was a single resonance at ca. 228−229 ppm. At higher loadings, a second resonance appeared at ca. 222 ppm. Figure 8 suggests that acetone may form complexes with different species present in the concentrated phosphoric acid solution that is the acidic component of SPA.

(51) Xu, T.; Munson, E. J.; Haw, J. F. *J. Am. Chem. Soc.* **1994**, *116*, 1962−1972.

Ab Initio Calculations. We used theoretical methods to model the complexation of either acetone or propene with some of the species expected to be present in a concentrated phosphoric acid solution. The acetone study was more detailed, because we were especially interested in trying to understand the large chemical shift of acetone on SPA. For the best imaginable calculation of this type, one would like to explicitly include several solvation shells of phosphoric and pyrophosphoric acid as well as long-range electrostatics, but this level of treatment is not currently feasible. Instead, we do what is most commonly done for calculations of adsorption on zeolites: use computationally manageable clusters to approximate the acid site and model interactions as if in the gas phase.

We considered the obvious cases of acetone complexed to either one phosphoric acid or one pyrophosphoric acid; as demonstrated below, we found two isomers of each. We also considered acetone complexed to two phosphoric acid molecules. A less obvious choice was acetone complexed to protonated phosphoric acid, $H_4PO_4^+$. We were motivated to consider the latter by the work of R. A. Munson, who carried out a detailed study of ionic equilibria in phosphoric acid.[52] Two equilibria were considered in that investigation, autoprotolysis

$$2H_3PO_4 \rightleftarrows H_4PO_4^+ + H_2PO_4^-$$

and self-dehydration

$$3H_3PO_4 \rightleftarrows H_3O^+ + H_4PO_4^+ + H_2P_2O_7^{2-}$$

Munson used cryoscopic and EMF measurements to determined the composition of 100% H_3PO_4 and obtained molal concentrations for the ionic species of $mH_4PO_4^+ = 0.54$, $mH_2PO_4^- = 0.26$, and $mH_3O^+ = mH_2P_2O_7^{2-} = 0.28$. Since 100% H_3PO_4 is formally 10.2*m* in itself, the concentration of $H_4PO_4^+$ reported by Munson corresponds to 5.3% of the phosphate groups. Ionic equilibria have not been quantified for phosphoric acid solutions more concentrated than 100% (P_2O_5 > 72.4%), and we are unable to cite a literature reference specifying the $H_4PO_4^+$ concentration expected for solutions in the concentration range of SPA. However, since SPA has a high concentration of pyrophosphoric acid, the following equilibrium should also be important.

$$2H_3PO_4 + H_4P_2O_7 \rightleftarrows 2H_4PO_4^+ + H_2P_2O_7^{2-}$$

Thus, although we are uncertain of the concentration of $H_4PO_4^+$ in SPA, we are satisfied that it is sufficiently high to warrant inclusion in the theoretical study.

In common with recent studies of adsorbates on zeolite Brønsted sites[53,54] we used density functional theory (DFT) to determine the geometries of various complexes of acetone or propene with phosphoric acids followed by ab initio chemical shift calculations using the gauge-invariant atomic orbital (GIAO) approach. All structures were calculated by using DFT with the B3LYP exchange-correlation functional and the 6-311+G(d,p) basis set. This level of theory has, in our experience, provided reliable models of hydrogen bonding and acid−base chemistry at manageable computational expense.

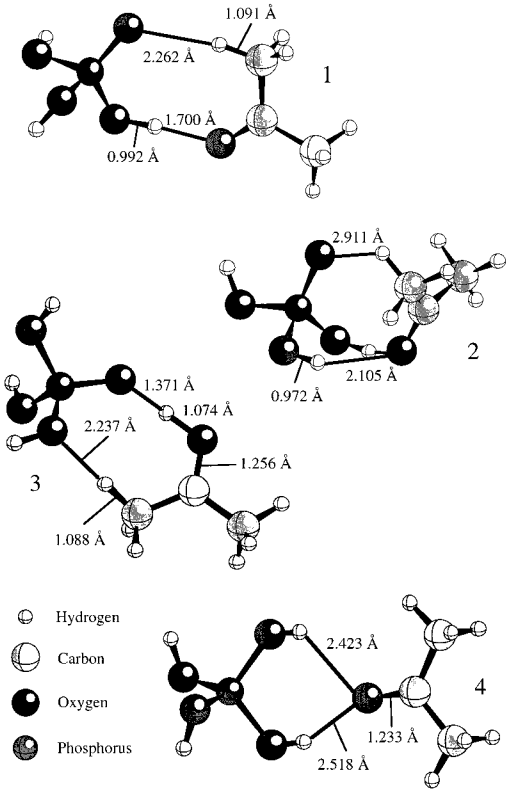

Figure 9. Complexes of acetone with one phosphoric acid molecule via one hydrogen bond (**1**) and two hydrogen bonds (**2**) and the complex of acetone with protonated phosphoric acid (**3** and **4**). Geometries were optimized at the B3LYP/6-311+G(d,p) level of theory.

The geometries of eight structures, modeling acetone on acidic species in SPA, are reported in Figures 9 and 10, and Figure 11 reports geometries of the lower energy structures modeling complexation of propene. Several additional structures were also calculated to obtain deprotonation energies, the energies of various thermodynamic reference states, or for chemical shift calculations. These included $H_4PO_4^+$, two isomers of H_3PO_4, the phosphoric acid dimer, two isomers of pyrophosphoric acid, the deprotonated states of the acids, acetone, protonated acetone, and propene. Geometries of these latter species as well as some higher energy complexes of acetone or propene not reported in Figures 9−11 are collected in the Supporting Information. Energies for the more important geometries, including thermal corrections, are compiled in Table 1.

The geometries in Figures 9 and 10 all show conventional hydrogen bonding between hydroxyl groups on phosphoric acid species and acetone. Structures **1** and **3** also suggest weak C−H−O hydrogen bonding. Structures **1** and **2** (Figure 9) are the two geometries we found for acetone hydrogen bonded to a single molecule of phosphoric acid. The monodentate geometry **1** was the most stable at −9.13 kcal/mol relative to isolated acetone and phosphoric acid at the same level of theory, and the bidentate structure **2** was less stable at −6.58 kcal/mol. We searched for other stable states including, for example, zwitterionic states of acetone and phosphoric acid, but these spontaneously reverted to the geometries shown. We also found two complexes with $H_4PO_4^+$; **3** was the more stable, but the bidentate structure **4** was only 5.60 kcal/mol higher. The oxygen−oxygen distance in structure **3**, 2.41 Å, indicates an exceptionally strong hydrogen bond. Also, the proton is closer to acetone than to phosphoric acid; this is the only species we observed for which proton transfer to acetone could be claimed. Partial proton transfer occurs although the proton affinity of

(52) Munson, R. A. *J. Phys. Chem.* **1964**, *68*, 3374−3377.
(53) Nicholas, J. B.; Haw, J. F.; Beck, L. W.; Krawietz, T. R.; Ferguson, D. B. *J. Am. Chem. Soc.* **1995**, *117*, 12350−12351.
(54) Beck, L. W.; Xu, T.; Nicholas, J. B.; Haw, J. F. *J. Am. Chem. Soc.* **1995**, *117*, 11594−11595.

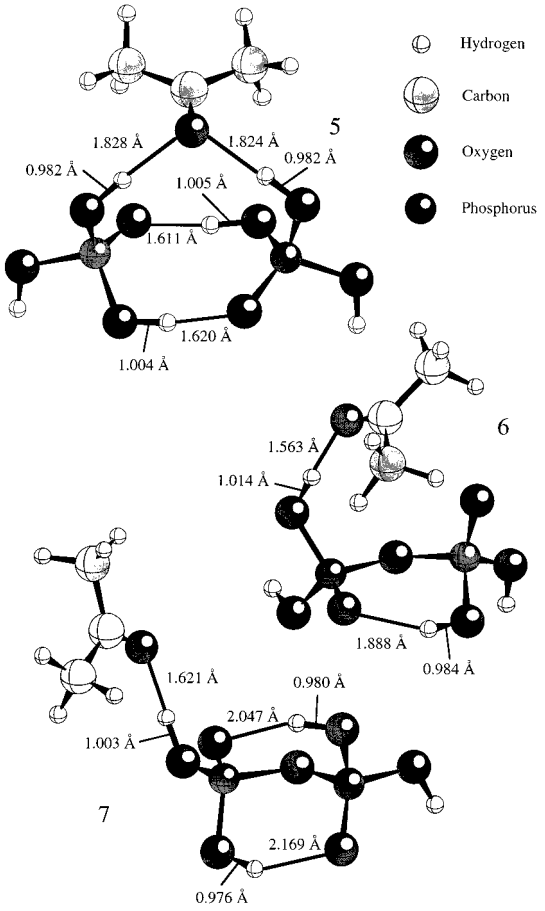

Figure 10. Complexes of acetone with either two molecules of phosphoric acid (**5**) or one of pyrophosphoric acid (**6** and **7**). Geometries were optimized at the B3LYP/6-311+G(d,p) level of theory.

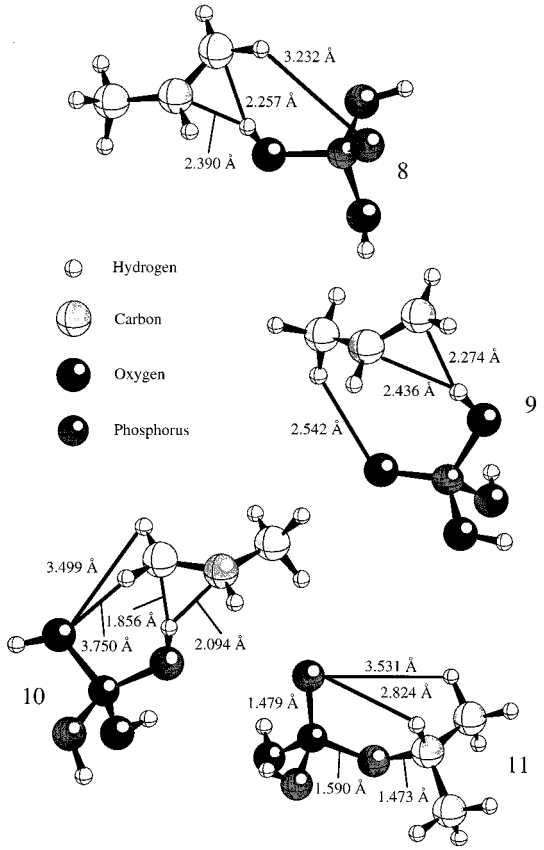

Figure 11. Complexes of propene with either phosphoric acid (**8** and **9**) or protonated phosphoric acid (**10**) and the reaction product isopropyl phosphate (**11**). Geometries were optimized at the B3LYP/6-311+G(d,p) level of theory.

isolated H_3PO_4 (198.0 kcal/mol at B3LYP/6-311+G(d,p)) is slightly higher than for isolated acetone at the same level of theory (195.5 kcal/mol).

Figure 10 reports the geometries we obtained for acetone with either two phosphoric acid molecules, **5**, or acetone with one molecule of pyrophosphoric acid, **6** and **7**. Species **5** is characterized by a chelated hydrogen bond, and there is precedent for such bonds in the literature.[55] We also searched for a geometry in which the phosphoric acid dimer formed a conventional two-center hydrogen bond to acetone, but we were unable to converge any such structure. We obtained structures for two 1:1 complexes of acetone and pyrophosphoric acid; calculations of 1:2 complexes were not attempted on the basis of the large computational resources necessary to obtain the smaller structures. **6** is the more stable species at −12.48 kcal/mol relative to the isolated molecules, but **7** is similar at −11.57 kcal/mol. Pyrophosphoric acid hydrogen bonds to acetone more strongly than does phosphoric acid; this is reflected in the reaction enthalpies as well as by the internuclear coordinates, and is also consistent with the relative gas-phase deprotonation energies of the acids.

We found four stable geometries with very similar energies for propene complexed with phosphoric acid. Figure 11 reports the structures of the two lowest energy species, **8** and **9**, while the other two are reported in the Supporting Information. We also found one complex between $H_4PO_4^+$ and propene **10**, which is also reported in Figure 11. All five propene complexes were characterized by a hydrogen bond between a hydroxyl group and the π cloud of the olefin. The optimized geometry of isopropyl phosphate **11**, known to be the reaction product between propene and phosphoric acid, is included in Figure 11 for completeness.

Chemical Shift Calculations. Chemical shift calculations provide a bridge between experimental measurements and theoretical geometries. We prefer the method of gauge-invariant atomic orbitals (GIAO) and Ahlrichs' basis sets for chemical shift calculations. As was found previously by other workers,[56,57] treatment of electron correlation with the GIAO-MP2 method of Gauss is essential for accurate ^{13}C chemical shifts for carbenium ions and related charged species. Unfortunately, GIAO-MP2 calculations rapidly become prohibitive with increasing numbers of basis functions. We obtained MP2/tzp/dz shifts for acetone, protonated acetone, propene, and complexes **1**−**4** and **8**−**11**, but the numbers of basis functions or primitives required for structures **5**−**7** exceeded the program limitations for ACES II, and these could not be obtained at MP2. However, we were able to calculate the ^{13}C shifts at GIAO-RHF/tzp/dz for all of **1**−**11**. Calculated shifts are reported in Table 2 for acetone complexes and Table 3 for propene complexes.

In common with our other recent work[58] we find that RHF shift calculations for the carbonyl carbon of acetone systematically overestimate the MP2 result. Previous work strongly

(55) Frisch, M. J.; Pople, J. A.; Del Bene, J. E. *J. Phys. Chem.* **1985**, *89*, 3664−3668.

(56) Xu, T.; Barich, D. H.; Torres, P. D.; Haw, J. F. *J. Am. Chem. Soc.* **1997**, *119*, 406−414.

(57) Xu, T.; Torres, P. D.; Barich, D. H.; Nicholas, J. B.; Haw, J. F. *J. Am. Chem. Soc.* **1997**, *119*, 346−405.

(58) Barich, D. H.; Nicholas, J. B.; Xu, T.; Haw, J. F. Theoretical Studies of the ^{13}C Chemical Shift Tensor of Acetone Complexed with Brønsted and Lewis Acids. In *J. Am. Chem. Soc.*, submitted for publication.

Table 1. Electronic Energies, Zero-Point Energies, and Thermal Corrections to Energies of Adsorption Complexes[a]

species and complexes	electronic energy[b]	ZPE[c]	thermal correction[d]	total energy[e]
Acet	−193.218179	0.084058	0.005425	−193.128696
Acet·H^+	−193.539655	0.096374	0.005413	−193.437868
H_3PO_4	−644.281722	0.048162	0.006313	−644.227247
$(H_3PO_4)_2$	−1288.601407	0.098237	0.013234	−1288.489936
$H_3PO_4 \cdot H_2PO_4^-$	−1288.097171	0.086860	0.012554	−1287.997757
$H_4P_2O_7$	−1212.106318	0.075028	0.009874	−1212.021416
$H_2PO_4^-$	−643.753473	0.036827	0.005658	−643.710988
$H_3P_2O_7^-$	−1211.616124	0.063897	0.009135	−1211.543092
$H_4PO_4^+$	−644.606086	0.059277	0.006331	−644.540478
H_3PO_4·Acet (**1**)	−837.517854	0.134598	0.012766	−837.370490
H_3PO_4·Acet (**2**)	−837.514107	0.135259	0.012415	−837.366433
$H_4PO_4^+$·Acet (**3**)	−837.876308	0.144526	0.012922	−837.718860
$H_4PO_4^+$·Acet (**4**)	−837.868218	0.145489	0.012797	−837.709932
$(H_3PO_4)_2$·Acet (**5**)	−1481.840734	0.186289	0.018870	−1481.635575
$H_4P_2O_7$·Acet (**6**)	−1405.347238	0.160708	0.016537	−1405.169993
$H_4P_2O_7$·Acet (**7**)	−1405.346300	0.161417	0.016335	−1405.168548
C_3H_6	−117.945586	0.080089	0.004073	−117.861424
$C_3H_6 \cdot H^+$	−118.243955	0.088458	0.004247	−118.151250
$H_3PO_4 \cdot C_3H_6$ (**8**)	−762.234433	0.129756	0.011975	−762.092702
$H_3PO_4 \cdot C_3H_6$ (**9**)	−762.234222	0.129863	0.011938	−762.092421
$H_4PO_4^+ \cdot C_3H_6$ (**10**)	−762.573519	0.140045	0.011841	−762.421633
i-$(C_3H_7)H_2PO_4$ (**11**)	−762.250797	0.133896	0.010284	−762.106617

[a] All energies reported are in hartrees. [b] Calculated at the B3LYP/6-311+G(d,p)//B3LYP/6-311+G(d,p) level of theory. [c] Zero-point energies were obtained without scaling at 298.15 K and 1 atm at the B3LYP/6-31G(d)//B3LYP/6-31G(d) level of theory. [d] Thermal corrections were calculated at 298.15 K and 1 atm at the B3LYP/6-31G(d)//B3LYP/6-31G(d) level of theory. [e] Total energy = E_0 + ZPE + thermal correction.

Table 2. Theoretical ^{13}C Isotropic Chemical Shifts[a] (ppm) for the C-2 Carbon of Acetone for Acetone, Protonated Acetone, and Acetone Complexes Formed with H_3PO_4, $H_4PO_4^+$, $(H_3PO_4)_2$, and $H_4P_2O_7$

	RHF-GIAO/tzp/dz// B3LYP/6-311+G(d,p)	MP2-GIAO/tzp/dz// B3LYP/6-311+G(d,p)
Acet	208.1	194.5
Acet·H+	263.7	256.8
H_3PO_4·Acet (**1**)	223.7	210.1
H_3PO_4·Acet (**2**)	228.7	215.4
$H_4PO_4^+$·Acet (**3**)	250.4	239.9
$H_4PO_4^+$·Acet (**4**)	241.0	229.9
$(H_3PO_4)_2$·Acet (**5**)	233.1	
$H_4P_2O_7$·Acet (**6**)	228.4	
$H_4P_2O_7$·Acet (**7**)	225.9	

[a] Isotropic chemical shifts are reported relative to TMS calculated at the same level of theory. The absolute shieldings (in ppm) of TMS are 193.2 for RHF and 198.7 for MP2.

Table 3. Theoretical ^{13}C Isotropic Chemical Shifts[a] (ppm) for Propene, Propene Complexed with H_3PO_4 and $H_4PO_4^+$, and Isopropyl Phosphate

		RHF-GIAO/tzp/dz// B3LYP/6-311+G(d,p)	MP2-GIAO/tzp/dz// B3LYP/6-311+G(d,p)
C_3H_6	C_1	120.4	115.1
	C_2	140.9	133.3
	C_3	19.7	21.8
$H_3PO_4 \cdot C_3H_6$ (**8**)	C_1	117.3	113.1
	C_2	152.2	143.8
	C_3	19.5	22.0
$H_3PO_4 \cdot C_3H_6$ (**9**)	C_1	131.8	117.2
	C_2	158.2	139.3
	C_3	32.9	21.9
$H_4PO_4^+ \cdot C_3H_6$ (**10**)	C_1	115.1	113.3
	C_2	166.3	156.9
	C_3	20.5	23.0
i-$(C_3H_7)H_2PO_4$ (**11**)	C_1	22.6	24.9
	C_2	66.9	76.7
	C_3	20.5	25.6

[a] Isotropic chemical shifts are reported relative to TMS calculated at the same level of theory. The absolute shieldings (in ppm) of TMS are 193.2 for RHF, and 198.7 for MP2.

suggests that MP2 shifts are reliable, even for "difficult" cases such as carbenium ions,[50,56,57] while RHF calculations are reliable for trends if not exact values. Acetone complexed to a single phosphoric acid yields MP2 shifts of 210.1 ppm for **1** and 215.4 ppm for **2**; these values are well below acetone in either SPA (up to ca. 231 ppm) or zeolite HZSM-5 (223 ppm). The structures for acetone complexed to $H_4PO_4^+$ have MP2 shifts of 239.9 and 229.9 ppm for **3** and **4**, respectively. These shifts bracket the largest experimental values for acetone on SPA.

Only RHF shift calculations were feasible for **5**−**7**, and these were interpreted relative to the RHF shifts for **1**−**4**. Complexation of acetone with two molecules of phosphoric acid, **3**, produces a slightly larger shift than complexation with one molecule of acid, **2**. Complexation with one molecule of pyrophosphoric acid, **6** and **7**, results in shifts little different from complexation with one phosphoric acid.

The results in Table 3 predict that C-2 of propene should show an appreciable downfield shift when dissolved in the acidic phase of SPA, but recall that we observed a value of 134 ppm, much closer to the gas-phase value. The calculated C-2 shift of isopropyl phosphate, 76.7 ppm, is in good agreement with the 80 ppm result in Figure 7.

Discussion

Solid phosphoric acid is more complex than phosphoric acid supported on a silica source. Chemical reactions occur in the preparation of SPA to form various silicon phosphate phases; thus the true support material in SPA is a mixture of crystalline reaction products. SPA does not contain Lewis sites, and the Brønsted acid sites on this catalyst arise from a viscous solution or glass (depending on temperature and composition) of phosphoric acid and phosphoric acid oligomers. The average chain length of these acids is strongly sensitive to preparation and handling of the catalyst and this accounts for the water sensitivity of SPA in commercial processes. The acidity of the phosphoric acid phase is not enhanced by the crystalline components.

The theoretical results in Figure 11 and Table 3 suggest that propene is not dissolved in the acidic phase of SPA at low temperatures, in agreement with our interpretation of in situ studies such as those in Figure 7. Complexation of propene with phosphoric acid or other, more acidic species in SPA should result in appreciable downfield shifts of the C-2 resonance, which are not observed. Propene is excluded from the glassy, acidic phase of SPA at low temperatures, and when it does enter SPA, at 273 K and above, it reacts to form isopropyl phosphate. The in situ NMR identification of isopropyl phosphate supports the classical mechanism for olefin oligomerization on SPA.[25] Ipatief was able to isolate phosphate esters using similar reaction conditions and showed that these produced oligomeric hydrocarbons upon heating.[59]

SPA is widely believed to be a weaker acid than zeolites, and we gave much thought to this comparison. The acid strength of SPA is a straightforward problem with a rigorous solution. The acid strengths of solutions and melts of phosphoric acid have been previously characterized over a very large concentration range by using the Hammett acidity function. At 298 K H_0 is -4.70 for 70% P_2O_5 and -6.96 for 85% P_2O_5.[60] Like other mineral acids, the Hammett acidity of phosphoric acid has a modest temperature dependence, becoming slightly larger (less negative) at higher temperatures. At 298 K our SPA samples have Hammett acidities in the range of -5 to -7. Although the acid strength of SPA does not approach that of 100% H_2SO_4 ($H_0 = -12$), SPA is unquestionably a strong acid.

Unfortunately, the Hammett formalism cannot be applied to zeolites with the same rigor as for phosphoric acid, but the comparison of acid strengths can be made in other ways. Experimental measurements of the deprotonation energies of zeolites are in the range of 284−318 kcal/mol,[61] and values near 296 kcal/mol are commonly used in theoretical studies to model isolated Brønsted sites.[62] The theoretical energies in Table 1 permit us to calculate the deprotonation energies of some of the species we used to model SPA; smaller values correspond to stronger acids. For a single phosphoric acid molecule in the gas phase the deprotonation energy is fairly large, 325.4 kcal/mol. However, the dimer of phosphoric acid has a value of 310.3 kcal/mol, indicating a significantly stronger acid than the monomer. Our calculations also show that a single pyrophosphoric acid is a strong gas-phase acid at 301.6 kcal/mol. We are unable to model a pyrophosphoric acid dimer, but consideration of the phosphoric acid dimer suggests that the deprotonation energy of the former would be well below the 296 kcal/mol value used to model zeolites theoretically. Not surprisingly, $H_4PO_4^+$ is a particularly strong acid with a deprotonation energy of 198.0 kcal/mol. While we are not able to fully model a concentrated phosphoric acid solution, the calculated deprotonation energies of the clusters considered here support the idea that SPA is a strong acid.

The geometries of the acetone complexes in Figures 9 and 10 show trends in the degree of proton transfer that generally reflect the deprotonation energies of the acids, which are in turn reflected in chemical shift trends. The MP2 shifts of the complexes of acetone with $H_4PO_4^+$, 239.9 ppm for **3** and 229.9 ppm for **4**, bracket the largest shift we observed for acetone on SPA, 231 ppm. We conclude that the acetone chemical shift reliably ranks the relative acid strengths of SPA and zeolites; SPA is the stronger acid.

On zeolites, propene is present either as free olefin, π complexes with the acid site, or lower concentrations of framework-bound alkoxyl species.[29,49] The latter species is analogous to the phosphate ester formed on SPA in that each is a covalently bound complex of propene and the acid site. The essential difference in the propene oligomerization activity of the two catalysts is the extent to which this intermediate forms. On the zeolite, the alkoxyl is reversibly formed as a minority species, and other propene molecules are available to react with it to form oligomers. On SPA, the reaction to form isopropyl phosphate is quantitative at 298 K. At higher temperatures, the ester is in equilibrium with olefin, and the position of this equilibrium moderates the oligomerization activity.

Conclusions

SPA is a supported liquid phase catalyst, a highly concentrated phosphoric acid solution on a support of crystalline silicon phosphate reaction products. The acid function of SPA is purely Brønsted in nature, and it is entirely due to the phosphoric acid phase—the crystalline component functions purely as a support. The acid strength of SPA exceeds that of typical zeolite catalysts; this is the reverse of the olefin oligomerization activity. Propene oligomerization proceeds through analogous intermediates on the two catalysts, but the phosphate ester formed on SPA is so stable that this reaction goes to completion and higher temperatures are required to establish an equilibrium with free olefin. The differential stabilities of the intermediates in propene oligomerization on zeolites vs SPA highlight an important aspect of catalysis: the more active catalysts avoid pathways with exceptionally stable intermediates.

Acknowledgment. The NMR component of this work was supported by the U.S. Department of Energy (DOE) Office of Basic Energy Sciences (BES) (Grant No. DE-FG03-93ER14354) and the theoretical component was supported by the National Science Foundation (CHE-9528959).

Supporting Information Available: Spectra of acetone adsorbed on SPA; structures of neutral and protonated acetone, propene, and phosphoric acid; structures of phosphoric acid related species; structures of complexes of propene and phosphoric acid; T_1 data for silicon phosphates; additional theoretical energies (6 pages print/PDF). See any current masthead page for ordering information and Web access instructions.

JA9813461

(59) Pines, H.; Ipatieff, V. N. *Catalytic Reactions at High Temperatures and Pressures*; Macmillan: New York, 1936.

(60) Rochester, C. H. *Acidity Functions*; Academic Press: New York, 1970.

(61) Datka, J.; Boczar, M.; Rymarowics, P. *J. Catal.* **1988**, *114*, 368−376.

(62) Brand, H. V.; Curtiss, L. A.; Iton, L. E. *J. Phys. Chem.* **1993**, *97*, 12773−12782.